

Shear-Driven Instabilities of Membrane Tubes and Dynamin-Induced Scission

Sami C. Al-Izzi^{1,2,3,4,*} Pierre Sens^{3,4} and Matthew S. Turner^{2,5}

¹*Department of Mathematics, University of Warwick, Coventry CV4 7AL, United Kingdom*

²*Department of Physics, University of Warwick, Coventry CV4 7AL, United Kingdom*

³*Institut Curie, PSL Research University, CNRS, Physical Chemistry Curie, F-75005, Paris, France*

⁴*Sorbonne Université, CNRS, UMR 168, F-75005, Paris, France*

⁵*Centre for Complexity Science, University of Warwick, Coventry CV4 7AL, United Kingdom*



(Received 13 October 2018; revised 21 October 2019; accepted 8 June 2020; published 1 July 2020)

Motivated by the mechanics of dynamin-mediated membrane tube fission, we analyze the stability of fluid membrane tubes subjected to shear flow in azimuthal direction. We find a novel helical instability driven by the membrane shear flow which results in a nonequilibrium steady state for the tube fluctuations. This instability has its onset at shear rates that may be physiologically accessible under the action of dynamin and could also be probed using *in vitro* experiments on membrane nanotubes, e.g., using magnetic tweezers. We discuss how such an instability may play a role in the mechanism for dynamin-mediated membrane tube fission.

DOI: [10.1103/PhysRevLett.125.018101](https://doi.org/10.1103/PhysRevLett.125.018101)

The covariant hydrodynamics of fluid membranes has been a subject of much interest in the soft matter and biological physics community in recent years, for both the general theoretical features of such systems [1–5] and their application to biological processes [6–9]. Such systems couple membrane hydrodynamics with bending elasticity and have been shown to display complex viscoelastic behavior in geometries with high curvature [10].

Membrane tubes are highly curved and are found in many contexts in cell biology, including the endoplasmic reticulum and the necks of budding vesicles [11]. Such tubes can be pulled from a membrane under the action of a localized force (such as from molecular motors) [12–14]. They are stable due to a balance between bending energy, involving the bending rigidity κ , and the surface tension σ with an equilibrium radius $r_0 = \sqrt{\kappa/2\sigma}$ [15].

One of the simplest ways to drive flows on the surface of these tubes is to impose a velocity in the azimuthal direction. The analysis of shape changes induced by such flows is the subject of this Letter. Two possible mechanisms for realizing such flows via *in vitro* and *in vivo* experiments are shown in Fig. 1.

The fission of membrane tubes plays an important role in many cellular processes, ranging from endocytosis to mitochondria fission [16,17]. The key component of the biological machinery required to induce membrane fission is a family of proteins called dynamin that hydrolyze Guanosine triphosphate (GTP) into Guanosine diphosphate [18,19]. Dynamin is a protein complex that oligomerizes to form polymers which wrap helically around membrane tubes [18,20,21]. Although there is clear evidence that dynamin undergoes a conformational change when it hydrolyzes GTP, there is not yet a consensus on the exact method of fission [22–26]. Recent coarse-grained

simulations have shed some light on the possible role of constriction and depolymerization [27]. It has been shown experimentally that, upon hydrolysis of GTP, dynamin (counter)rotates rapidly while constricting [19], giving a mechanism for the generation of flows in the azimuthal direction. Another possible way of driving such flows is by pulling a narrow membrane (nano)tube from either a giant unilamellar vesicle (GUV) or a cell using magnetic tweezers. Magnetic field oscillations can then be used to spin the attached magnetic bead [28–30], thereby setting up a frictional flow in the tube.

The membrane behaves as a viscous fluid with 2D viscosity η_m . The Saffman-Delbrück length, $L_{SD} = \eta_m/\eta$ [31–33], with η the bulk fluid viscosity, is the distance over which bulk hydrodynamics screens membrane flows in planar geometry. In the case of a membrane tube the screening length is modified due to geometric effects and becomes $\sqrt{L_{SD}r_0}$, [33]. We consider dynamics on a scale less than this, such that the dominant dissipation mechanism involves the membrane flows. This means that we can neglect bulk flows on sufficiently short length scales (short tubes) [9,34]. For further details, see Supplemental Material (SM) [35].

We consider a lipid membrane as a manifold equipped with metric g_{ij} and second fundamental form b_{ij} [36]. The coordinate basis is defined by the triad $\{\vec{e}_1, \vec{e}_2, \vec{n}\}$ where \vec{e}_i and \vec{n} are the basis of the tangent bundle and normal bundle of the surface, respectively. The surface has velocity $\vec{V} = \mathbf{v} + w\vec{n}$, where $\mathbf{v} = v^i\vec{e}_i$. We label vectors in the membrane tangent space in bold, e.g., \mathbf{x} , and vectors in \mathbb{R}^3 with arrows, e.g., \vec{x} . We define the mean and Gaussian curvature as $2H = b^i_i$ and $K = \det b^i_j$, respectively. We assume the membrane behaves like a zero-Reynolds

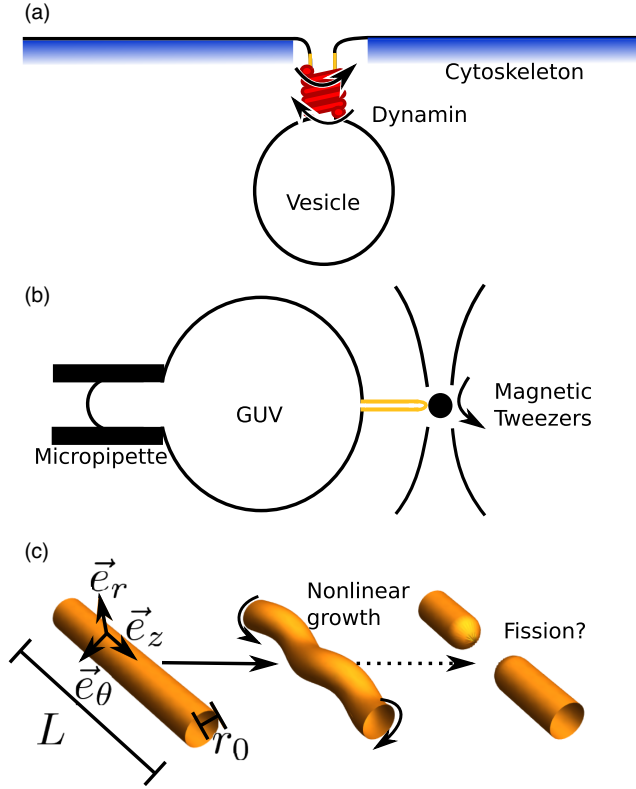


FIG. 1. Possible realizations of shear-driven instabilities on membrane tubes (shown in orange throughout). (a) Dynamin on the neck of a budding vesicle. The protein constricts and (counter)rotates, prior to fission of the tube. This rotation drives a significant shear flow near the neck of the vesicle. We discuss the possible effects of the Gaussian curvature of the neck in the conclusion. (b) A GUV with membrane tube pulled by magnetic tweezers; the magnetic bead can be spun in order to drive flows in the azimuthal direction on the tube. (c) Sketch of the growth of the helical instability described in this Letter. The final stage is a possible pathway to tube fission due to nonlinear effects. The basis vectors on the membrane \vec{e}_i , where $i = r, \theta, z$, length of tube L , and equilibrium radius r_0 , are labeled. Middle panel shows shear direction.

number fluid in the tangential direction [37] and has bending energy given by the usual Helfrich energy [38]. Surface tension σ is treated as a Lagrange multiplier imposing membrane area conservation. We will assume zero spontaneous curvature for simplicity. For conciseness we will simply state the equations of motion for the membrane; for details on their derivation, see Refs. [7,39] or SM [35].

The continuity equation for an incompressible membrane is given by

$$\nabla_i v^i = 2Hw, \quad (1)$$

which is simply the Euclidean continuity equation modified to account for the normal motion of the membrane [7,40].

Force balance normal to the membrane means the normal elastic and viscous forces must sum to zero, leading to the following:

$$\begin{aligned} & \kappa[2\Delta_{LB}H - 4H(H^2 - K)] + 2\sigma H \\ & + 2\eta_m[b^i_j \nabla_i v^j - 2(2H^2 - K)w] = 0. \end{aligned} \quad (2)$$

Here κ is the bending rigidity of the membrane and Δ_{LB} is the Laplace-Beltrami operator. Note that we are using a geometrical definition of Δ_{LB} that is analogous to a curl-curl operator on a manifold, hence the sign difference with the usual Laplacian operator in the shape equation (see SM for details [35]). This is a modified form of the shape equation first derived by Zhong-Can and Helfrich [15], but with the addition of viscous normal forces given by fluid flow on the membrane. The term coupling the second fundamental form and gradients in tangential velocity can be thought of as the normal force induced by fluid flowing over an intrinsically curved manifold. This term is of fundamental importance in the present study as it drives a shape instability. The other nonstandard term, $\sim(2H^2 - K)w$, is the dissipative force associated with the normal velocity, inducing flows in the tangential direction on a curved surface.

Force balance in the tangential direction gives

$$\eta_m[\Delta_{LB}v^i - 2Kv^i + 2(b^{ij} - 2Hg^{ij})\nabla_j w] - \nabla^i \sigma = 0, \quad (3)$$

which is the modified form of the 2D Stokes equations. The new terms, coupling Gaussian curvature with tangential velocity, and curvature components with the gradients in normal velocity, come from the modified form of the rate-of-deformation tensor which accounts for the curved and changing geometry of the membrane. The term $\sim Kv^i$ describes the convergence or divergence of streamlines on a curved surface. The term $\sim(b^{ij} - 2Hg^{ij})\nabla_j w$ describes the forces induced tangentially by the dynamics of the membrane.

We consider a ground-state membrane tube ($w = 0$) of length L in cylindrical coordinates (r, θ, z) with radius $r_0 = \sqrt{\kappa/2\sigma_0}$ and impose a velocity $v = v_0\vec{e}_\theta$ at $z = 0$ (which can be interpreted as the edge of an active dynamin ring, for example). Making use of the azimuthal symmetry the continuity and Stokes equations reduce to an Ordinary differential equation that admits the solution

$$\mathbf{v}^{(0)} = (v_0 - \Omega z) \frac{1}{r_0} \vec{e}_\theta, \quad (4)$$

where the exact value of the shear flow Ω depends on the boundary condition at $z = L$, but roughly scales as $\Omega \sim v_0/L$ if we either implement torque balance, e.g., at the boundary where a tube joins onto a planar membrane, or simply set $v(L) = 0$; see SM for more details [35].

We can now make a perturbation about this ground state in $r(z, \theta, t) = r_0 + u(\theta, z, t)$, $\mathbf{v} = \mathbf{v}^{(0)} + \delta v^\theta(\theta, z, t)\vec{e}_\theta + \delta v^z(\theta, z, t)\vec{e}_z$, $\sigma = \sigma_0 + \delta\sigma(\theta, z, t)$, and $w = \partial_t u$. Making use of the discrete Fourier transform, $f(\theta, z, t) = \sum_{q,m} \tilde{f}_{q,m}(t)e^{iqz+im\theta}$, where $\tilde{f}_{q,m}$ is the discrete Fourier

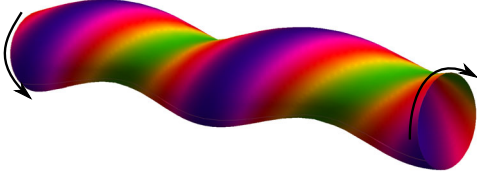


FIG. 2. The normal component of the viscous force per unit area on a helical shaped tube coming from the term $\eta_m b^i_j \nabla_i v^j$ in Eq. (2) (purple outward, green inward). This shows the helical nature of the instability above the critical shear rate. The tube would eventually be advected to stability again, as the helix winds up under the shear flow (see text), although the tube may reach the nonlinear deformation regime before this happens.

transform of $f(\theta, z)$ with $m \in \mathbb{Z}$ and $q = 2\pi n/L$ where $n \in \mathbb{Z} \setminus \{0\}$, we can write Eqs. (1)–(3) in Fourier space and linearize in the perturbations. The linear response of the normal force balance is the following:

$$\begin{aligned} \mathcal{F}_{q,m}^u \bar{u}_{q,m} + \mathcal{F}_{q,m}^\sigma \bar{\delta\sigma}_{q,m} + \mathcal{F}_{q,m}^\theta \bar{\delta v}^\theta_{q,m} \\ + \mathcal{F}_{q,m}^z \bar{\delta v}^z_{q,m} + \mathcal{G}_{q,m} \bar{\delta w}_{q,m} = 0, \end{aligned} \quad (5)$$

where $\mathcal{F}_{q,m}^u = (4\sigma_0^2/\kappa)[\tilde{q}^4 + m^4 + 2\tilde{q}^2 m^2 - 2m^2 + 1] - (2\eta_m m \tilde{q} \Omega / r_0^2)$, $\mathcal{F}_{q,m}^\sigma = 1/r_0$, $\mathcal{F}_{q,m}^\theta = (2\eta_m \eta_m / r_0^2)$, $\mathcal{F}_{q,m}^z = 0$, and $\mathcal{G}_{q,m} = (2\eta_m / r_0^2)$, where $\tilde{q} = qr_0$.

Note that the sign of the final term in the $\mathcal{F}_{q,m}^u$ coefficient, scaling with the shear Ω , suggests that the shear flow could lead to an instability in the $m \neq 0$ modes; see Fig. 2. Note that the $(m \rightarrow -m, \tilde{q} \rightarrow -\tilde{q})$ symmetry of the normal force defines a ‘‘handedness’’ which changes upon reversing the direction of the shear rate.

Similar linear response equations can be found for the force balance and continuity in the tangential directions; these can then be used to solve for $\bar{\delta v}^z_{q,m}$, $\bar{\delta v}^\theta_{q,m}$, and $\bar{\delta\sigma}_{q,m}$ in terms of $\bar{u}_{q,m}$ and its time derivative. From this we derive the following growth rate equation for $\bar{u}_{q,m}$, where time is normalized according to $t = \tilde{t}\tau$, with $\tau = \eta_m/\sigma_0$,

$$\partial_{\tilde{t}} \bar{u}_{q,m} = -im \frac{v_0 \eta_m}{r_0 \sigma_0} \bar{u}_{q,m} - \tilde{\Omega} m \partial_{\tilde{q}} \bar{u}_{q,m} + F(q, m) \bar{u}_{q,m}, \quad (6)$$

where

$$\begin{aligned} F(q, m) = \{m\tilde{q}[(m^2 + \tilde{q}^2)^2 - 2\tilde{q}^2] \tilde{\Omega} \\ - (m^2 + \tilde{q}^2)^2 [1 + m^4 + \tilde{q}^4 + 2m^2(\tilde{q}^2 - 1)]\} (2\tilde{q}^4)^{-1} \end{aligned} \quad (7)$$

and $\tilde{\Omega} = \eta_m \Omega / \sigma_0$ is the dimensionless shear.

The modes become unstable when the real part of the growth rate changes sign to $\text{Re}\{F(m, q)\} > 0$, which occurs for

$$\tilde{\Omega} m \tilde{q} > \frac{(m^2 + \tilde{q}^2)^2 [1 + m^4 + \tilde{q}^4 + 2m^2(\tilde{q}^2 - 1)]}{(m^2 + \tilde{q}^2)^2 - 2\tilde{q}^2}. \quad (8)$$

The $m = 0$ peristaltic mode is always linearly stable. This is not the case for the $m = 1$ mode, which is the first to

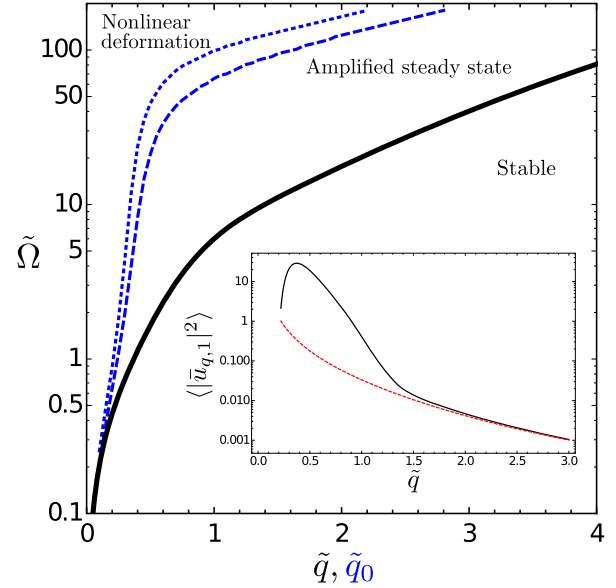


FIG. 3. Dynamical phase diagram of the state of the tube in the presence of fluctuations. Helical \tilde{q} modes to the left of the black line are unstable according to Eq. (8). The blue dashed and blue dotted lines show the value of $\tilde{\Omega}$ for which 5% and 32% of the fluctuations become nonlinear as a function of \tilde{q}_0 , the cutoff on the noise spectrum coming from the finite tube length. Inset: The statistical steady state of $\langle |\bar{u}_{q,1}|^2 \rangle$ for cutoff $\tilde{q}_0 = 0.2$ and shear $\tilde{\Omega} = 1$ in black with equilibrium thermal fluctuations shown in dashed red.

be driven unstable. The stability threshold for the $m = 1$ mode is plotted in Fig. 3 in solid black. Note that the growth rate is a discrete function of $\tilde{q} = (2\pi n r_0 / L)$ with discretization set by the length of the tube. This means that, beyond a certain rotation speed, a helical mode will grow, with pitch length initially set by the length of the tube. The apparent divergence of the growth rate for small \tilde{q} is ultimately limited by bulk hydrodynamics.

This analysis is complicated by the advection in \tilde{q} space of helical modes that arises from the term involving $\partial_{\tilde{q}}$ in Eq. (6). This reflects the fact that the ground-state shear flow continuously adds new turns to an existing helix, thereby increasing its characteristic wave number. Large wave numbers are stable, so a helical perturbation rendered unstable by the shear flow is eventually stabilized by this advection. This leads to a nonequilibrium steady state, which can be obtained by solving Eq. (6) with thermal noise added using the method of stochastic characteristics; see SM [35] and Ref. [41] for details. This nonequilibrium steady state for $\langle |\bar{u}_{q,m}|^2 \rangle$ has a peak in q space; see Fig. 3 inset. Because the $m = 1$ modes are critical in the $\tilde{q} \rightarrow 0$ limit [42] we choose a small \tilde{q} cutoff for the noise spectrum at $\tilde{q}_0 = 2\pi r_0 / L$, which is physical, given the finite length of our tube. Equation (6) is based on a small perturbation expansion and breaks down when the spatial gradients become large, $\langle |\nabla u|^2 \rangle \sim 1$, in which case the end state

might be quite different. In Fig. 3, we plot the value of $\tilde{\Omega}$, as a function of the cutoff \tilde{q}_0 , for which 5% and 32% of fluctuations are in the nonlinear regime as the blue dashed and blue dotted lines. Beyond this shear rate the tube will be deformed nonlinearly and it is not clear if there will be a steady state. A full analysis of this is beyond the scope of the present work.

In the small \tilde{q} limit, the threshold shear [Eq. (8)] is $\tilde{\Omega} \approx 2\tilde{q}$ (see SM [35]). The shear rate is $\Omega \sim (2\pi r_0 \nu / L)$, where ν is the spinning frequency. Assuming that the cutoff wave number of the tube is associated with a fundamental mode $\tilde{q}_0 = (2\pi r_0 / L)$ gives the critical spinning frequency for the onset of instability as $\nu_{\text{crit}} \simeq (2\sigma_0 / \eta_m)$. The functional form of the critical frequency can be understood using a scaling analysis of Eq. (2); see SM [35].

Typical membranes in the fluid (liquid disordered) phase have viscosities $\eta_m \sim 10^{-9}$ – 10^{-8} Pa m s [43] (higher in the liquid ordered phase). However, much higher values of effective viscosity have been associated with tubes pulled from living cells, $\eta_m \sim 10^{-7}$ – 10^{-5} Pa m s [8]. We use these numbers, noting that effective viscosities may be higher still if the neck is crowded with proteins. We assume the surface tension takes a physiologically typical value [44] of $\sigma_0 \sim 10^{-5}$ N m⁻¹ [18,22]. Vesicular necks correspond to short tubes with $\tilde{q}_0 \sim 1$, so from Fig. 3 we find $\tilde{\Omega} \sim 5$ for the stability criterion and $\tilde{\Omega} \sim 50$ for the nonlinearity criterion which correspond to $\nu \sim 5$ – 500 Hz and $\nu \sim 50$ – 5000 Hz, respectively, with the wide range traced to the uncertainty in membrane viscosity. Dynamin polymers have been measured to have rotational frequencies $\nu \sim 10$ Hz [19], suggesting the instability could be accessible to dynamin for the higher values of viscosity found in cells. These estimates are quite conservative as in a realistic scenario active fluctuations are likely to be much larger than thermal fluctuations, perhaps by an order of magnitude or more, and we are unlikely to have such a hard cutoff at \tilde{q}_0 .

A natural way for the fluctuations to progress in the nonlinear regime is fission of the tube, which is of particular significance given that the exact mechanism for dynamin-mediated fission is unknown. As the fluctuations grow the surface tension will increase, either narrowing the tube or causing pearling [45]. An increase in tension has been shown to accelerating spontaneous tube fission [46] and friction impeding membrane flow has been shown experimentally to scission tubes [47]. The increase in fluctuations is also likely to promote the formation of hemifused states, which can be an important intermediate for fission [27]. Surface tension fluctuations, even at the linear level, can be estimated to be much larger than the ground-state surface tension and this could also be important in driving membrane lysis; see SM [35]. This picture of fission, promoted by membrane hydrodynamics just outside the active dynamin site, is consistent with the experimental observation that the location of fission is near the edge of the active dynamin site rather than directly

under it [46]. The timescale over which the instability grows is of the order of $\tau \sim 10^{-2}$ – 1 s, which is sufficiently fast to be consistent with the dynamin-induced fission process [48].

Although we have provided evidence that a membrane instability can be driven by the rotation of dynamin, our study is based on the simplified geometry of a cylindrical tube, rather than the neck of a budding vesicle, a location where dynamin might typically act *in vivo*. While our approach becomes analytically intractable for such complex membrane geometries, we can gain some intuition into how the driving force per unit area of the instability changes with the geometry of the neck region by considering the term in the normal force balance equation that is responsible for driving the instability. Given the helical symmetry of the instability we infer that this driving force per unit area goes like the mixed derivative in the shape $f_{\text{driving}} \sim \eta_m b^i_j \nabla_i v^j$. The term which acts like the shear rate on the tube now depends on z and we must calculate it numerically; see SM [35]. In the case of a catenoidal neck this leads to an amplification of the driving force by (only) a factor of 2 near the active site ($z = 0$); for details see SM [35]. While a relatively small effect, this is qualitatively consistent with the experimental observation that dynamin fission of a tube *in vitro* often occurs near the GUV neck [46] and that fission on the necks of budding vesicles *in vivo* occurs faster than it does on long tubes [22,49].

A second possibility for the nonlinear growth is a stable nonequilibrium shape driven by the membrane flow. In this case it is worth noting an analogy between the membrane tube instability discussed here and elastic rods under torsion that deform nonlinearly into plectonemes [50]. If excess membrane area is more readily available it may be possible for the unstable tube to develop *fluid* plectonemes if the instability develops without a scission-inducing increase in tension. Similar structures are observed in experiments on long tubes covered in dynamin [19,49].

The experiment suggested in Fig. 1(b) would both test our predictions more quantitatively and probe the nonlinear evolution of the fluctuations so as to determine whether these hydrodynamic effects alone are sufficient to induce fission. The instability should also arise in a longer tube; however, the quantitative nature of our predictions would likely require modifications due to screening of membrane flow by the ambient fluid. In this case we expect that the unstable wavelength would then be set by the screening length $\sqrt{L_{\text{SD}} r_0}$ rather than the tube length [33,51] and that our results would continue to hold at the scaling level.

In summary, we have developed a hydrodynamic theory that predicts an instability on fluid membrane tubes that is driven purely by a shear in the membrane flow. Such flows are shown to first drive a helical instability, which is quite distinct from any previously identified instabilities of fluid membrane tubes. This instability, although eventually advected to stability by the flow, is shown to be able to

significantly modify and enhance the fluctuation spectra of a membrane tube. We predict that this instability, and perhaps its fully nonlinear manifestation, may be physiologically accessible to dynamin. Such hydrodynamic effects have not previously been considered in models of its function [49,52]. This instability may provide a mechanism for dynamin-mediated tube scission.

The authors acknowledge very helpful comments from S. Ramaswamy (Bangalore) and helpful discussions with P. Bassereau (Institut Curie), R. Phillips (CalTech), and J. E. Sprittles, G. Rowlands, and J. Binysh (Warwick). S. C. A.-I. would like to acknowledge funding from the UK EPSRC under Grant No. EP/L015374/1, the Centre for Doctoral Training in Mathematics for Real-World Systems, and support from the Labex CeTisPhyBio (ANR-11-LABX-0038, ANR-10-IDEX-0001-02).

*Present address: School of Physics and EMBL-Australia node in Single Molecule Science, University of New South Wales, Sydney 2052, Australia.

- [1] W. Cai and T. C. Lubensky, *Phys. Rev. Lett.* **73**, 1186 (1994).
- [2] W. Cai and T. C. Lubensky, *Phys. Rev. E* **52**, 4251 (1995).
- [3] J.-B. Fournier, *Int. J. Nonlinear Mech.* **75**, 67 (2015).
- [4] A. Sahu, R. A. Sauer, and K. K. Mandadapu, *Phys. Rev. E* **96**, 042409 (2017).
- [5] A. Sahu, A. Glisman, J. Tchoufag, and K. K. Mandadapu, *Phys. Rev. E* **101**, 052401 (2020).
- [6] P. Sens, *Phys. Rev. Lett.* **93**, 108103 (2004).
- [7] M. Arroyo and A. DeSimone, *Phys. Rev. E* **79**, 031915 (2009).
- [8] F. Brochard-Wyart, N. Borghi, D. Cuvelier, and P. Nassoy, *Proc. Natl. Acad. Sci. U.S.A.* **103**, 7660 (2006).
- [9] R. G. Morris and M. S. Turner, *Phys. Rev. Lett.* **115**, 198101 (2015).
- [10] M. Rahimi, A. DeSimone, and M. Arroyo, *Soft Matter* **9**, 11033 (2013).
- [11] M. Kaksonen and A. Roux, *Nat. Rev. Mol. Cell Biol.* **19**, 313 (2018).
- [12] I. Derényi, F. Jülicher, and J. Prost, *Phys. Rev. Lett.* **88**, 238101 (2002).
- [13] A. Yamada, A. Mamane, J. Lee-Tin-Wah, A. Di Cicco, C. Prvost, D. Lvy, J.-F. Joanny, E. Coudrier, and P. Bassereau, *Nat. Commun.* **5**, 3624 (2014).
- [14] D. Cuvelier, I. Derényi, P. Bassereau, and P. Nassoy, *Biophys. J.* **88**, 2714 (2005).
- [15] Ou-Yang Zhong-can and W. Helfrich, *Phys. Rev. A* **39**, 5280 (1989).
- [16] S. J. McClure and P. J. Robinson, *Molecular membrane biology* **13**, 189 (1996).
- [17] S. Frank, B. Gaume, E. S. Bergmann-Leitner, W. W. Leitner, E. G. Robert, F. Catez, C. L. Smith, and R. J. Youle, *Dev. Cell* **1**, 515 (2001).
- [18] B. Antonny, C. Burd, P. De Camilli, E. Chen, O. Daumke, K. Faelber, M. Ford, V. A. Frolov, A. Frost, J. E. Hinshaw, T. Kirchhausen, M. M. Kozlov, M. Lenz, H. H. Low, H. McMahon, C. Merrifield, T. D. Pollard, P. J. Robinson, A. Roux, and S. Schmid, *EMBO J.* **35**, 2270 (2016).
- [19] A. Roux, K. Uyhazi, A. Frost, and P. De Camilli, *Nature (London)* **441**, 528 (2006).
- [20] A. Roux, G. Koster, M. Lenz, B. Sorre, J.-B. Manneville, P. Nassoy, and P. Bassereau, *Proc. Natl. Acad. Sci. U.S.A.* **107**, 4141 (2010).
- [21] R. Shlomovitz, N. S. Gov, and A. Roux, *New J. Phys.* **13**, 065008 (2011).
- [22] A. Roux, *F1000Prime Rep.* **6**, 86 (2014).
- [23] M. M. Kozlov, *Biophys. J.* **77**, 604 (1999).
- [24] M. M. Kozlov, *Traffic* **2**, 51 (2001).
- [25] Z. A. McDargh, P. Vázquez-Montejo, J. Guven, and M. Deserno, *Biophys. J.* **111**, 2470 (2016).
- [26] Z. A. McDargh and M. Deserno, *Traffic* **19**, 328 (2018).
- [27] M. Pannuzzo, Z. A. McDargh, and M. Deserno, *eLife* **7** (2018) <https://doi.org/10.7554/eLife.39441>.
- [28] F. H. C. Crick and A. F. W. Hughes, *Exp. Cell Res.* **1**, 37 (1950).
- [29] B. G. Hosu, M. Sun, F. Marga, M. Grandbois, and G. Forgacs, *Phys. Biol.* **4**, 67 (2007).
- [30] M. Monticelli, D. V. Conca, E. Albisetti, A. Torti, P. P. Sharma, G. Kidiyoor, S. Barozzi, D. Parazzoli, P. Ciarletta, M. Lupi, D. Petti, and R. Bertacco, *Lab Chip* **16**, 2882 (2016).
- [31] P. G. Saffman and M. Delbruck, *Proc. Natl. Acad. Sci. U.S.A.* **72**, 3111 (1975).
- [32] P. G. Saffman, *J. Fluid Mech.* **73**, 593 (1976).
- [33] M. L. Henle and A. J. Levine, *Phys. Rev. E* **81**, 011905 (2010).
- [34] F. Bahmani, J. Christenson, and P. Rangamani, *Continuum Mech. Thermodyn.* **28**, 503 (2016).
- [35] See Supplemental Material at <http://link.aps.org/supplemental/10.1103/PhysRevLett.125.018101> for detailed calculations.
- [36] T. Frankel, *The Geometry of Physics: An Introduction*, 3rd ed. (Cambridge University Press, Cambridge, England, 2011).
- [37] J. Happel and H. Brenner, in *Low Reynolds Number Hydrodynamics: With Special Applications to Particulate Media*, 1st ed., Mechanics of Fluids and Transport Processes Vol. 1, edited by M. Nijhoff (Kluwer Boston, The Hague, Boston, 1983).
- [38] W. Helfrich, *Z. Naturforsch.* **28C**, 693 (1973).
- [39] P. Rangamani, A. Agrawal, K. K. Mandadapu, G. Oster, and D. J. Steigmann, *Biomech. Model. Mechanobiol.* **12**, 833 (2013).
- [40] J. Marsden and T. Hughes, *Mathematical Foundations of Elasticity*, Dover Civil and Mechanical Engineering Series (Dover Publications, Inc., New York, 1994).
- [41] P.-L. Chow, *Stochastic Partial Differential Equations* (Chapman and Hall/CRC, Boca Raton, FL, 2014).
- [42] J.-B. Fournier and P. Galatola, *Phys. Rev. Lett.* **98**, 018103 (2007).
- [43] T. T. Hormel, S. Q. Kurihara, M. K. Brennan, M. C. Wozniak, and R. Parthasarathy, *Phys. Rev. Lett.* **112**, 188101 (2014).
- [44] Noting that this value may vary enormously near the neck of a budding vesicle subject to forces, e.g., from neighboring actomyosin.
- [45] P. Nelson, T. Powers, and U. Seifert, *Phys. Rev. Lett.* **74**, 3384 (1995).

- [46] S. Morlot, V. Galli, M. Klein, N. Chiaruttini, J. Manzi, F. Humbert, L. Dinis, M. Lenz, G. Cappello, and A. Roux, *Cell* **151**, 619 (2012).
- [47] M. Simunovic, J.-B. Manneville, H.-F. Renard, E. Evergren, K. Raghunathan, D. Bhatia, A. K. Kenworthy, G. A. Voth, J. Prost, H. T. McMahon, L. Johannes, P. Bassereau, and A. Callan-Jones, *Cell* **170**, 172 (2017).
- [48] S. Dar, S. C. Kamekar, and T. J. Pucadyil, *Nat. Cell Biol.* **17**, 1588 (2015).
- [49] S. Morlot, M. Lenz, J. Prost, J.-F. Joanny, and A. Roux, *Biophys. J.* **99**, 3580 (2010).
- [50] B. Audoly and Y. Pomeau, *Elasticity and Geometry: From Hair Curls to the Non-linear Response of Shells* (Oxford University Press, Oxford, England, 2010).
- [51] J. H. Ferziger and M. Peric, *Computational Methods for Fluid Dynamics*, 3rd ed. (Springer-Verlag, Berlin, 2002).
- [52] M. Lenz, J. Prost, and J.-F. Joanny, *Phys. Rev. E* **78**, 011911 (2008).